Thermo X https://doi.org/10.70401/tx.2026.0023

Supplementary information

Simultaneously improving thermal conductivities and mechanical strength of carbon fibers/epoxy composites *via* CNT/copolymer hybrid interphase

Yuhan Lin, Wenqing Zhang, Hua Guo, Jiawen Liu, Junliang Zhang, Yongqiang Guo, Junwei Gu

S1. Characterization

Fourier transform infrared (FT-IR) spectra of the samples were measured on Bruker Tensor 27 (Bruker Co., Germany) through the ATR module. X-ray diffraction (XRD) curves of the samples were obtained on D8 DISCOVER A25 XRD equipment (Bruker Co., Germany) equipped with a Co target radiation source with a scanning speed of 5°/min. X-ray photoelectron spectroscopy (XPS) analyses of the samples were carried out by Kratos Axis Ultra DLD equipment (Kratos Corp., UK). Size exclusion chromatography (SEC, PL-GPC50, Agilent Technologies, Inc., USA) was used to determine the number average molar mass (M_n), weight average molar mass (M_w), and molar mass distribution ($Đ$) of the samples using Dimethylformamide (DMF, HPLC grade) as the elution solvent at a flow rate of 1.0 mL/min. Scanning electron microscopy (SEM) images were captured on a Verios G4 equipment (FEI Co., USA).Atomic force microscopy (AFM) images of the samples were collected by a Dimension Fast Scan AFM (Bruker Corp., Germany). Dynamic contact angle test of the samples was recorded by a dynamic contact angle meter and a tensiometer (Data Physics Instruments DCAT 21, Germany) through immersing CF into two different testing liquid including deionized water and diiodomethane, with the immersion height of 5 mm. Flexural strength and interlaminar shear strengths (ILSS) of the composites were measured using an Electron Omnipotence Experiment Machine CMT 7204 (Shenzhen New Sansi Co., China) according to the standard of ASTM D 7264 and ASTM D 2344. Tensile strengths of the composites were measured using an Electron Omnipotence Experiment Machine CMT 5105 (Shenzhen New Sansi Co., China) according to the standard of ASTM 3039. For each sample, measurements were repeated three times, and the average result was used to calculate the average value and the standard deviation. Thermal conductivity coefficient (λ) values of the samples were measured using 7577 F1 probe under block module by Hot Disk TPS2200 thermal constant analyzer (AB Co., Sweden), with the sample size of 20 mm×20 mm×1.5 mm according to the standard of ISO 2207-2: 2022. The direction of heat flow for internal ($\lambda_{/\!/}$) and interfacial ($\lambda_{\perp}$) are shown in **Figure S5**. For each sample, measurements were repeated three times, and the average result was used to calculate the average value and the standard deviation. The density and specific heat parameters of the sample were determined by the static hydrostatic weighing method and the differential scanning calorimetry method, and the test results are shown in **Table S2-3**. Infrared thermal images were captured by Ti 300 infrared thermography (Fluke Co., USA). The composites were placed on the surface of a 100 °C constant-temperature DRB-3/3D flatbed thermal platform (Tianjin Taisite Instrument Co., Ltd.) and heated, and then infrared thermal images were taken. Thermogravimetric analyses (TGA) of the samples were carried out by STA 499F3 (NETZSCH Corp., Germany) at 10°C/min (Nitrogen atmosphere), over temperature range of 50~800 °C. Dynamic mechanical analyses

(DMA) of the samples were carried out with heating rate of 2 °C/min and frequency of 1 Hz using Q800 (TA Instruments Co., USA). The electrical conductivities of the samples were obtained by RTS-8 (Guangzhou Four Probes Technology Co., China). The electromagnetic interference (EMI) shielding performance of the samples was measured by an MS4644A Vector Network Analyzer instrument (Anritsu Co., Japan) using the wave-guide method in X-band (8.2~12.4 GHz) according to ASTM D5568-2008, and the corresponding dimension was 22.86×10.16×1.5 mm^3. The reflection (S_{11}) and transmission parameters (S_{21}) obtained from the results were used to calculate the SE_T, SE_A, and SE_R according to the following equations:

$$SE_R\ (dB) = -10\log_{10}(1-|S_{11}|^2)$$

$$SE_A\ (dB) = -10\log_{10}\left(\frac{|S_{21}|^2}{1-|S_{11}|^2}\right)$$

$$SE_T\ (dB) = SE_R + SE_A$$

The heat conduction and electromagnetic wave energy loss behaviors of composites were simulated by COMSOL Multiphysics 6.1 software. Wireless charging test was conducted by placing the composite between the iPhone 14 Pro mobile phone (Apple Inc., United States) and the wireless charger (Black Shark Co., China), which was aligned with the wireless charging coil. The charging standard used was Qi2.

S2. Supplementary figures

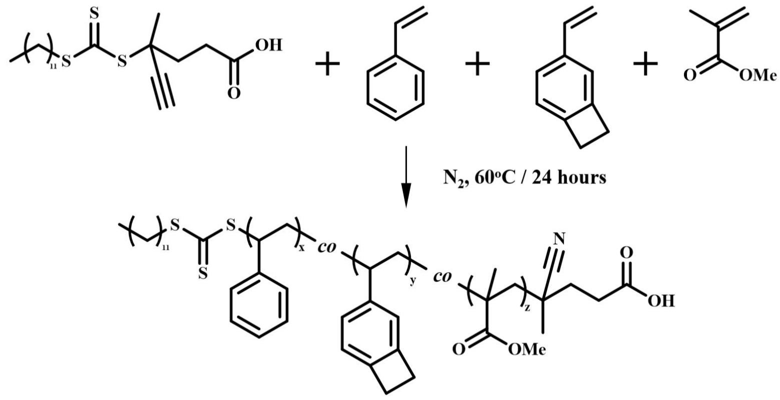

Scheme S1. Synthetic scheme of P(S-*co*-BCB-*co*-MMA).

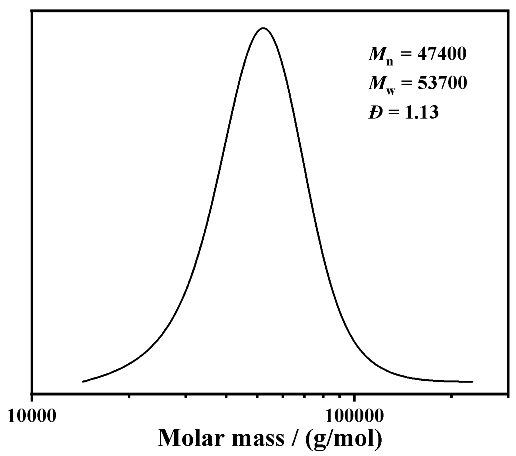

Figure S1. SEC curve of P(S-*co*-BCB-*co*-MMA).

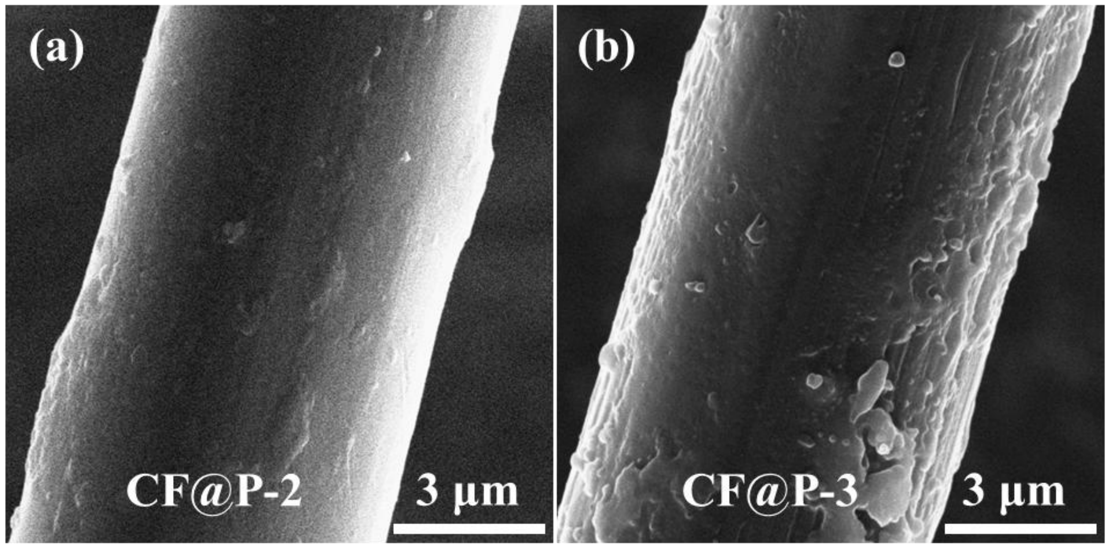

Figure S2. SEM images of CF@P-2~3.

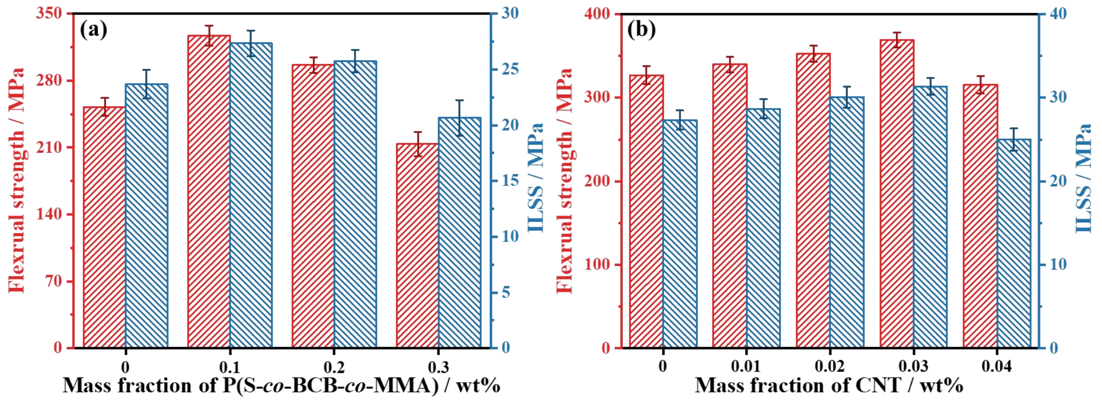

Figure S3. The flexural strength and ILSS test results of CF, CF@P-1~3 (a) and CF@(CNT/P)-1~4 (b) after being composed with epoxy resin.

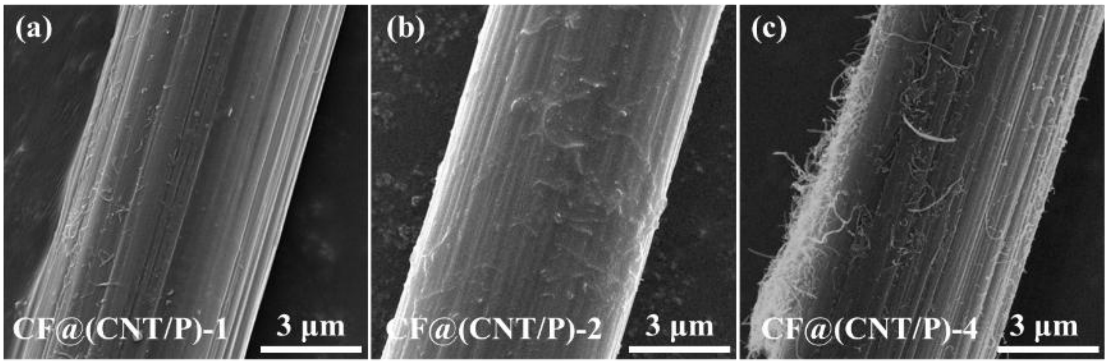

Figure S4. SEM images of CF@(CNT/P)-1, CF@(CNT/P)-2, CF@(CNT/P)-4.

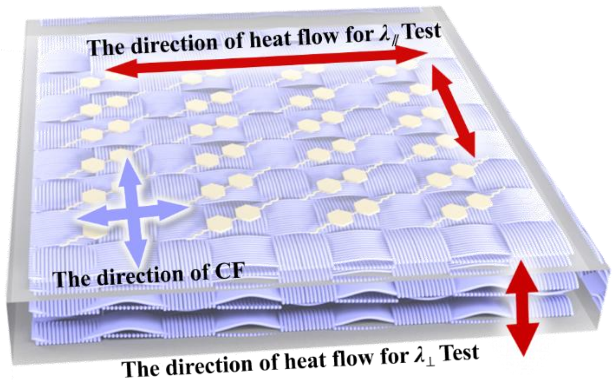

Figure S5. The direction of heat flow for $\lambda_{/\!/}$ and $\lambda_{\perp}$.

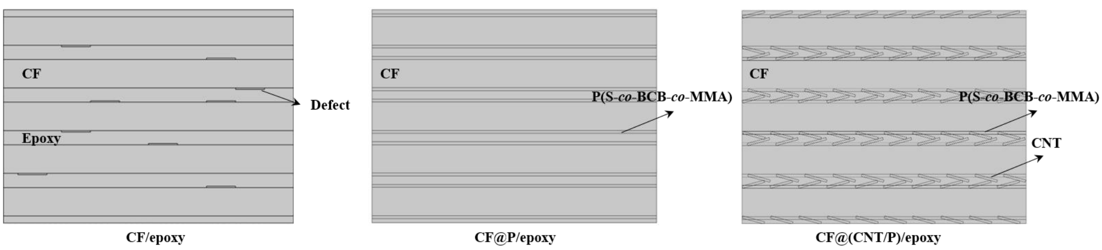

Figure S6. Microscopic model for finite element simulation.

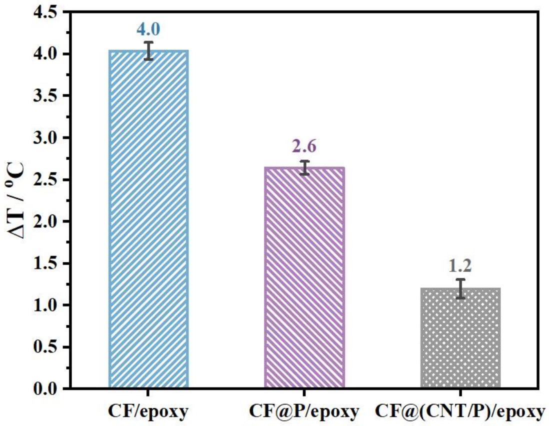

Figure S7. The temperature difference at the interface between CF and epoxy in finite element simulation for different composites.

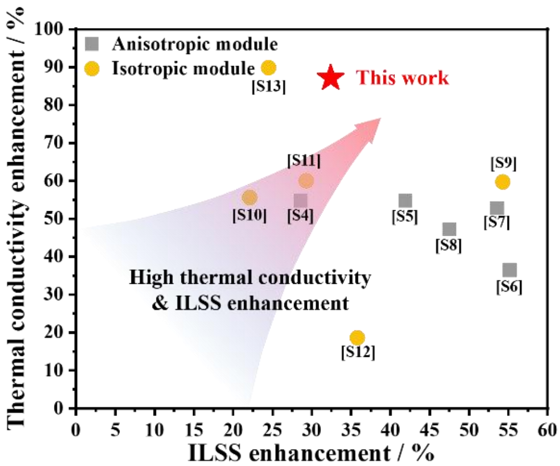

Figure S8. Thermal conductivity and ILSS enhancement between the CF@(CNT/P)/epoxy composite and other modification methods for CF reinforced composites in literature.

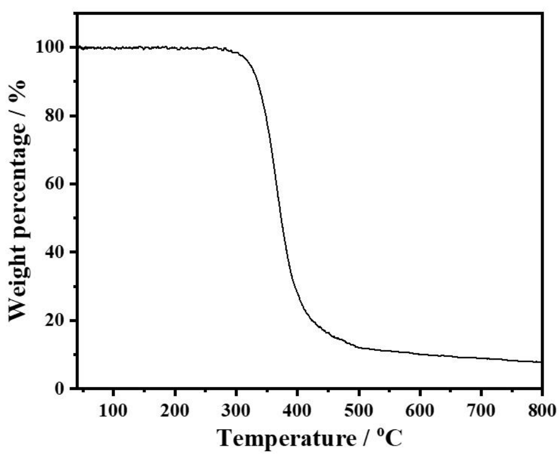

Figure S9. TGA curve of epoxy matrix.

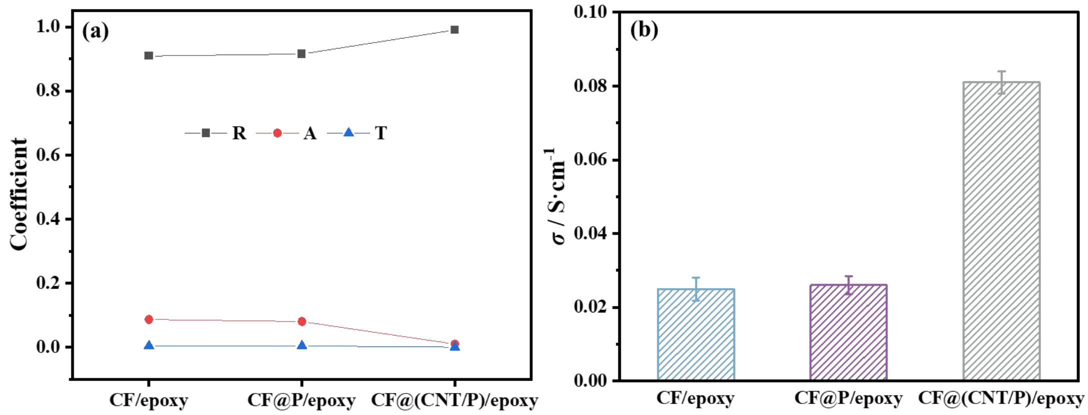

Figure S10. The electromagnetic wave reflection, absorption and transmission rates (a) and the electrical conductivity (b) of CF/epoxy, CF@P/epoxy, and CF@(CNT/P)/epoxy composites.

S3. Supplementary tables

Table S1. Elemental ratios of CF, CF@P, and CF@(CNT/P).

Samples	Concentrations of elements/%		O/C
	C	O	
CF	84.80	15.20	0.18
CF@P	77.37	22.63	0.29
CF@(CNT/P)	80.31	19.69	0.25

Table S2. The specific heat capability and density of the samples in the thermal conductivity test.

Samples	Specific heat capability (J/(g·K))	Density (g/cm^3)
CF/epoxy	1.00	1.58
CF@P/epoxy	0.97	1.59
CF@(CNT/P)/epoxy	0.93	1.57

Table S3. The specific heat capability, density, $\lambda_{//}$ and $\lambda_{\perp}$ of the CF/epoxy composite prepared without LCE.

Parameter	Specific heat capability (J/(g·K))	Density (g/cm^3)	$\lambda_{//}$ (W/(m·K))	$\lambda_{\perp}$(W/(m·K))
Value	1.06	1.55	6.81	0.27

Table S4. Parameters of FEM for heat conduction[1-3].

Model parameters		Values				
Physical parameters	environmental temperature	20 °C				
	bottom heat source temperature	100 °C				
	thermal insulation	on both the left and right sides				
	heating time	1 ms				
	model size	60 μm × 45 μm				
Material parameters		CF	epoxy	P(S-*co*-BCB-*co*-MMA)	CNT	Air
	thermal conductivity (W/(m·K))	10.5	0.25	0.16	3000	0.025
	specific heat capability (J/(g·K))	0.74	1.26	1.20	0.80	1.006
	density (g/cm^3)	1.80	1.10	1.05	0.20	0.001

Table S5. Thermal conductivity and ILSS enhancement between the CF@(CNT/P)/epoxy composite and other modification methods for CF reinforced composites.

Samples	*λ// enhancement / %*	*λ⊥enhancement / %*	*ILSS enhancement / %*	*Ref.*
CF@(CNT/P)/epoxy	*41.0*	*87.1*	*32.4*	*This work*
L_2S_1-CF felt/EP	*58.1*	*54.7*	*28.6*	*[S4]*
PFM@CF felt/EP	*28.2*	*54.7*	*41.9*	*[S5]*
MXene/PDA/PCF/EP	*2.6*	*36.4*	*55.2*	*[S6]*
CF@SnO_2/EP	--	*52.8*	*53.6*	*[S7]*
UCF-Z_{125}/PEEK	--	*47.2*	*47.5*	*[S8]*
CF/PDA/CNF/PVA/CNT/EP	*59.7 (isotropic)*		*54.3*	*[S9]*
CF@GnPs	*55.6 (isotropic)*		*22.1*	*[S10]*
0.5%-CF@BPEN/PEEK	*60.0 (isotropic)*		*29.3*	*[S11]*
CNTs/CF/PEEK	*18.6 (isotropic)*		*35.8*	*[S12]*
Graphene/CF/PPBESK	*89.8 (isotropic)*		*24.5*	*[S13]*

Table S6. Thermal characteristic data of CF/epoxy, CF@P/epoxy, and CF@(CNT/P)/epoxy composites.

Samples	Weightless temperature/°C		T_{HRI}/°C	T_g/°C
	5%	30%		
CF/epoxy	360.0	430.2	197.0	127.8
CF@P/epoxy	363.7	431.1	198.0	131.1
CF@(CNT/P)/epoxy	368.5	435.5	200.3	139.1

Table S7. Parameters of FEM for electromagnetic field[S2, S3, S14].

Model parameters		Values				
Physical parameters	input power at the upper port	1 W/m				
	port type	rectangular port				
	ideal conductor	on both the left and right sides				
	model size	60 μm × 45 μm				
Material parameters	electrical conductivity (S/cm)	CF	Epoxy	P(S-*co*-BCB-*co*-MMA)	CNT	Air
		6250	1×10^{-12}	1×10^{-14}	1×10^{7}	1×10^{-16}

Table S8. Parameters of FEM for waveguide.

Model parameters		Values
Physical parameters	waveguide size	22.86 mm × 10.16 mm × 150 mm
	port type	rectangular port
	ideal conductor	the wall of the waveguide
	input power at the upper port	1 W
Material parameters	based on the results of the electrical conductivity test	

S3. Supplementary reference

S1.Zhang S-C, Lu X-H, Liu J, Wu J, Jia X, Sun B, et al. A biomimetic thermal conduction network enables metal-level thermal conductivity in polymer nanocomposites. ACS Nano. 2025;19(41):36663-36674. [DOI: 10.1021/acsnano.5c12250]

S2.Tang L, Zhang J, Gu J. Random copolymer membrane coated pbo fibers with significantly improved interfacial adhesion for PBO fibers/cyanate ester composites. Chin J Aeronaut. 2021;34(2):659-668. [DOI: 10.1016/j.cja.2020.03.007]

S3.Ren C, Gui X, Wang Y, Xiang L, Tang B, Shi S, et al. Preparation of ag@cfc/ep composites with excellent thermal management performance via electroless silver plating on polydopamine-modified carbon fiber/carbon felt. Compos Commun. 2025;58:102552. [DOI: 10.1016/j.coco.2025.102552]

S4.Li S, Jin Y, Wang Z, He Q, Chen R, Wang J, et al. Preparation and characterisation of nickel -plated carbon fibre/polyether ether ketone composites with high electromagnetic shielding and high thermal conductivity. Colloid Polym Sci. 2019;297(7):967-977. [DOI: 10.1007/s00396-019-04522-5]

S5.Luo J, Xue Y, Yang X, Yang C, Jiang M, Zhang L, et al. Integrating thermal, emi shielding, and mechanical properties in carbon fiber/epoxy resin composites via interface-layup synergistic design. Adv Funct Mater. 2026;36(8):e13660. [DOI: 10.1002/adfm.202513660]

S6.Yao X, Yang G, Chen J, Zhao Q, Jiang J. Enhancing mechanical, emi shielding, and thermal properties of pitch-based carbon fiber composites via mxene/polydopamine modification. Polym Compos. 2025;46(16):14883-14898. [DOI: 10.1002/pc.30097]

S7.Zhou J, Zhu B, Zhang X, Zhang Y, Yuan X, Zhou M, et al. High-performance and multifunctional heterostructured carbon fiber@sno2 nanosheet reinforced peek composites for electromagnetic interference shielding and thermal conductivity. Nano Res. 2025;18(8):94907562. [DOI: 10.26599/NR.2025.94907562]

S8.Zhou J, Zhu B, Zhao W, Zhang Y, Zhu A, Di C, et al. Pomegranate-like znmn2o4 nanospheres/carbon fiber network for interface enhancement structure-function peek

composites with good electromagnetic interference shielding and thermal conductivity. Compos Commun. 2024;50:102015. [DOI: 10.1016/j.coco.2024.102015]
S9.Quan G, Wu Y, Li W, Li D, Liu X, Wang K, et al. Construction of cellulose nanofiber/carbon nanotube synergistic network on carbon fiber surface to enhance mechanical properties and thermal conductivity of composites. Compos Sci Technol. 2024;248:110454. [DOI: 10.1016/j.compscitech.2024.110454]
S10.Wang F, Cai X. Improvement of mechanical properties and thermal conductivity of carbon fiber laminated composites through depositing graphene nanoplatelets on fibers. J Mater Sci. 2019;54(5):3847-3862. [DOI: 10.1007/s10853-018-3097-3]
S11.Zeng X, Shi X, Lin Y, Zhu W, Li H, Zhang J, et al. Improved interfacial compatibility of carbon fibers/peek laminated composites via incorporating biphenyl-branched poly(aryl-ether-nitrile). Journal of Materials Science & Technology. 2026;255:259-269. [DOI: 10.1016/j.jmst.2025.09.003]
S12.Leow C, Kreider P B, Sommacal S, Kluth P, Compston P. Electrical and thermal conductivity in graphene-enhanced carbon-fibre/peek: The effect of interlayer loading. Carbon. 2023;215:118463. [DOI: 10.1016/j.carbon.2023.118463]
S13.Wang B, Li N, Cheng S, Hu F, Li G, Guo H, et al. Thermal conductivity and mechanical properties enhancement of CF/PPBESK thermoplastic composites by introducing graphene. Polym Compos. 2022;43(5):2736-2745. [DOI: 10.1002/pc.26570]
S14.Liu A, Xu X, Qiu H, Guo H, He M, Yu Z, et al. Bioinspired hollow heterostructure fillers for enhanced electromagnetic interference shielding in polyimide aerogels. InfoMat. 2025;7(11):e70060. [DOI: 10.1002/inf2.70060]